Membrane Fusion Induced by a Short Fusogenic Peptide Is Assessed by Its Insertion and Orientation into Target Bilayers†

Isabelle Martin,*,‡,§ Eve-Isabelle Pécheur,*,§,|| Jean-Marie Ruysschaert,‡ and Dick Hoekstra||

Laboratoire de Chimie-Physique des Macromolécules aux Interfaces (LCPMI), Université Libre de Bruxelles, Bvd du Triomphe, CP 206/2, B-1050 Bruxelles, Belgium, and Department of Physiological Chemistry, University of Groningen, Antonius Deusinglaan 1, 9713 AV Groningen, The Netherlands

Received December 16, 1998; Revised Manuscript Received April 2, 1999

ABSTRACT: To clarify the molecular mechanism by which an amphipathic negatively charged peptide consisting of 11 residues (WAE) induces fusion, and the relevance of these features for fusion, its mode of insertion and orientation into target bilayers were investigated. Using attenuated total reflection Fourier transform infrared spectroscopy (ATR-FTIR) in combination with techniques based on tryptophan fluorescence, the peptide was found to form an α-helix, shallowly inserted into the membrane to which it is anchored. Interestingly, in the presence of target membranes, WAE inserts into the target bilayer as an α-helix oriented almost parallel to the lipid acyl chains. The accessibility of the peptide to either acrylamide (as an aqueous quencher of Trp fluorescence) or deuterium oxide (on the course of an FTIR deuteration kinetics) was lower in the presence than in the absence of target membranes, confirming that under those conditions, the peptide was shielded from the aqueous environment. Since fusion experiments have shown a temperature dependence, the effect of this later parameter on the structure and mode of insertion of the peptide was also analyzed. In the presence of target membrane, but not in their absence, the amount of α-helical structure increased with temperature, reflecting a similar temperature-dependent increase in the rate and extent of WAE-induced fusion. Also, the extent of penetration of the helix into the target membrane was greater at 37 °C than at lower temperatures. This temperature-dependent distinction was revealed by a decreased accessibility of the peptide to deuterium oxide and acrylamide at 37 °C as compared to that at lower temperatures. These data underscore the role of peptide structure, peptide penetration, and orientation in the mechanism of protein-induced membrane fusion.

Processes such as endo- or exocytosis, membrane recycling, fertilization, and infection by enveloped viruses require one or more critical membrane fusion reactions. Yet, fusion is an energetically unfavorable event since biological membranes are submitted to strong repulsive hydration, electrostatic, and static barriers (*1*, *2*). These barriers can be overcome by membrane proteins, which facilitate local dehydration (*3*) and are thought to induce local perturbations in the lipid bilayer through their insertion into membranes (*1*, *4*). A key feature in viral and cellular fusion phenomena is the involvement of specific fusion proteins, of which the viral spike glycoproteins responsible for penetration of enveloped viruses into their host cells (*5*, *6*) and sperm proteins involved in sperm−egg fusion have been characterized (*7*, *8*). Considerable progress has been made over the past few years in defining the actors and events that drive fusion. In particular, extensive work has focused on the role of short segments of relatively hydrophobic residues, commonly found in a membrane-anchored polypeptide chain, and termed fusion peptides. This stretch of residues is susceptible to interacting with and destabilizing a lipid bilayer (*9*−*13*).

With respect to insight into the molecular mechanism underlying the overall fusion event, large voids are still apparent. Several model systems have thus been developed to simulate protein-mediated fusion. These include synthetic peptides corresponding to the putative fusion segment, which are commonly added to model membranes (such as liposomes) as free monomers (*9*−*13*). A major drawback of these systems is their poor significance as truly membrane fusion-mimicking systems, since the peptides are dissociated from their normal membrane-anchored environment. To more closely simulate membrane fusion induced by a membrane-bound protein, we have developed in recent studies a model system consisting of an 11-mer synthetic peptide, called WAE (N-Trp-Ala-Glu-Ser-Leu-Gly-Glu-Ala-Leu-Glu-Cys), covalently anchored to a liposomal surface (*14*, *15*). The fusion properties of WAE are strictly dependent on its membrane anchorage. Previous investigations by Fourier transform infrared spectroscopy (FTIR)[1] revealed that anchorage causes the peptide to fold into an α-helical structure, thought to be required for fusion, whereas WAE in its free form exhibits an extended β-sheet conformation (*15*). These

† We acknowledge the financial support obtained from the ARC (Actions de Recherches Concertées) and the European Commission (Contract BIO4-CT97-2191). E.-I.P. was a recipient of a fellowship from the European Commission (Contract BMH4-98-5056), and I.M. is a scientific collaborator of the National Fund for Scientific Research (Belgium).

* To whom correspondence should be addressed. I.M.: fax, 32-2-650-53-82; e-mail, imartin@ulb.ac.be. E.-I.P.: fax, 31-50-363-2728; e-mail, e.Pecheur-huet@med.rug.nl.

‡ Université Libre de Bruxelles.

§ These authors contributed equally to this work.

|| University of Groningen.

10.1021/bi9829534 CCC: $18.00
Published on Web 06/24/1999

studies were carried out in the absence of target vesicles, i.e., at nonfusogenic conditions. Here, we have investigated the structural and functional features of WAE in a model system consisting of peptide-coupled PC/chol donor vesicles and PS/PE (10:3) as target membranes. Using this system, we were able to demonstrate a direct relationship between the temperature dependence of fusion and the ability of the peptide to adopt an α-helical structure and to penetrate into the target membrane. The role and significance of peptide conformation and orientation during the fusion process are discussed.

MATERIALS AND METHODS

Chemicals

Egg yolk phosphatidylcholine (PC), L-α-dipalmitoylphosphatidylethanolamine (DPPE), cholesterol (chol), and dipicolinic acid (pyridine-2,6-dicarboxylic acid, DPA) were obtained from Sigma. $TbCl_3 \cdot 6H_2O$ (99.9% pure) was from ACROS Organics. Bovine brain phosphatidylserine (PS) and phosphatidylethanolamine (PE) were purchased from Avanti Polar Lipids. *N*-Succinimidyl 3-(2-pyridyldithio)propionate (SPDP)-derivatized DPPE (PE-PDP) was synthesized as described previously (H. Martin, 1990). The fluorescent lipid analogues *N*-(7-nitro-2,1,3-benzoxadiazol-4-yl)phosphatidylethanolamine (*N*-NBD-PE) and *N*-(lissamine rhodamine B sulfonyl)phosphatidylethanolamine (*N*-Rh-PE) were purchased from Molecular Probes. All other reagents were of analytical grade.

Preparation of Liposomes

All liposomes were prepared by sonication followed by extrusion, as described in ref *14*. Their average diameter was 100−150 nm. Peptide-coupled liposomes, termed donor liposomes throughout the work, consisted of PC/chol/PE-PDP (3.5:1.5:0.25). Coupling was obtained by an overnight conjugation of the peptide WAE (N-Trp-Ala-Glu-Ser-Leu-Gly-Glu-Ala-Leu-Glu-Cys-OH) with liposomes (PE-PDP/peptide molar ratio of 1:5). Uncoupled peptide was eliminated by gel filtration through a Sephadex G-25 column (PD-10 column, Pharmacia). Target liposomes were composed of PS/PE or DOPS/DOPE (molar ratio of 10:3). The phospholipid concentration was measured by the method of Mrsny (*16*).

Assays for Monitoring Vesicle Fusion

Lipid mixing was assayed as described by Struck et al. (*17*). PS/PE target vesicles were added to a suspension of peptide-coupled liposomes containing *N*-NBD-PE and *N*-Rh-PE (1 mol % each) in 10 mM Tris and 150 mM NaCl (pH 7.4) at a lipid molar ratio of 1:1 or 6:1 (total lipid concentration of 70 μM). The increase in NBD fluorescence was monitored at 37 °C (unless indicated otherwise) as a function of time in a SPF 500 Aminco fluorimeter (λ_{exc} = 460 nm, λ_{em} = 534 nm) under continuous stirring. Zero percent and 100% fluorescence were taken as the intrinsic fluorescence intensity of NBD/Rh-labeled liposomes and the fluorescence obtained after addition of 0.2% Triton X-100 (final concentration), corrected for detergent-induced quenching of NBD fluorescence, respectively.

Internal contents mixing was assayed by using the $TbCl_3$/DPA assay as described in ref *18*.

Tryptophan Fluorescence Quenching by Aqueous Quenchers

Emission spectra of the peptide-coupled liposomes suspended in 10 mM Tris and 150 mM NaCl (pH 7.4) were recorded as a function of temperature between 300 and 400 nm at a λ_{exc} of 295 nm, in the absence or presence of target vesicles. The spectra were corrected for the vesicle blank (scatter) and for the dilution caused by the addition of liposomes. Trp fluorescence measurements were taken in the absence and presence of acrylamide, which acts as a collisional quencher of Trp (*15*). The quenching data were analyzed with the Stern−Volmer plot using the equation $F_0/F = 1 + K_{sv}[Q]$, where F_0 and F are the fluorescence intensities at 340 nm in the absence and presence of a given acrylamide concentration [Q], respectively, and K_{sv} is the Stern−Volmer quenching constant. In the case of acrylamide quenching, a deviation from linearity was observed in Stern−Volmer plots. This deviation indicates the existence of two Trp populations, one accessible to quenching and the other inaccessible or buried. Data were then analyzed according to the modified Stern−Volmer equation (*19*):

$$F_0/\mathrm{DF} = 1/fK_{sv}[Q] + 1/f$$

where F_0 is the fluorescence intensity in the absence of quencher, DF is the fluorescence decrease due to quenching, K_{sv} and [Q] are as described above, and $f = F_{0a}/(F_{0a} + F_{0b})$ which is the fraction of the initial fluorescence which is accessible to the quencher (F_{0a} and F_{0b} are the contributions of the accessible and buried fluorophores, respectively).

Attenuated Total Reflection Fourier Transform Infrared Spectroscopy (ATR-FTIR)

Spectra were recorded at room temperature on a Bruker IFS55 FTIR spectrophotometer equipped with a liquid nitrogen-cooled mercury cadmium telluride (MCT) detector at a nominal resolution of 2 cm^{-1}, and encoded every 1 cm^{-1}. The spectrophotometer was continuously purged with air, which had been dried on a silica gel column (5 cm × 130 cm). The internal reflection element was a germanium plate (50 mm × 50 mm × 2 mm, Harrick EJ2121) with an aperture angle of 45°, yielding 25 internal reflections. For each spectrum, 532 scan cycles were averaged; in each cycle, the sample spectra were rationed against the background spectra of a clean germanium plate. For polarization experiments, a Bruker gold wire grid polarizer was positioned before the sample and the reference.

Oriented multilayers were obtained by slow evaporation of the donor liposomes in the absence or in the presence of target vesicles under an N_2 stream and at different temper-

[1] Abbreviations: PC, phosphatidylcholine; PS, phosphatidylserine; PE, phosphatidylethanolamine; DPPE, L-α-dipalmitoylphosphatidylethanolamine; DOPS, dioleoylphosphatidylserine; DOPE, dioleoylphosphatidylethanolamine; chol, cholesterol; DPA, pyridine-2,6-dicarboxylic acid; PE-PDP, *N*-succinimidyl 3-(2-pyridyldithio)propionate-derivatized DPPE; PElys, lysine coupled to L-α-dipalmitoylphosphatidylethanolamine; *N*-NBD-PE, *N*-(7-nitro-2,1,3-benzoxadiazol-4-yl)phosphatidylethanolamine; *N*-Rh-PE, *N*-(lissamine rhodamine B sulfonyl)-dihexadecanoyl-*sn*-glycero-3-phosphoethanolamine; ATR-FTIR, attenuated total reflection Fourier transform infrared spectroscopy.

atures (10, 20, and 37 °C) on one side of the germanium plate (*16*). The ATR plate was then sealed in a universal sample holder and hydrated by flushing with ^{2}HO-saturated for 2 h. During this period of time, only the readily accessible peptide bonds are exchanged. Importantly, the random structure shifts from about 1655 to about 1640 cm^{-1} upon H−^{2}H exchange, allowing differentiation of the α-helix from random structures (*21*). It must be noted that during the preparation of the semidry film, many hydration water molecules are not removed (*22*). This explains why the secondary structure of the protein is usually not modified.

Secondary Structure Determination. The determination of the secondary structure was based on the vibrational bands of protein or peptide, and particularly the amide I band (1600−1700 cm^{-1}), which is sensitive to the secondary structure (*23*). This amide I band located in a region of the spectrum often free of other bands is composed of 80% pure C═O vibration (*24*). The analysis was performed on the amide I region of deuterated samples because hydrogen−deuterium exchange allows differentiation of accessible α-helix and irregular structures, the absorption band of which shifts from ∼1655 to 1642 cm^{-1} (*20*, *21*). Fourier self-deconvolution was carried out using a Lorentzian line shape for the deconvolution and a Gaussian line shape for the apodization. To quantify the area of the different components of amide I revealed by self-deconvolution, a least-squares iterative curve fitting was performed to fit Lorentzian line shapes to the spectrum between 1700 and 1600 cm^{-1}. To avoid introducing artifacts due to the self-deconvolution procedure, the fitting was performed on the non-deconvoluted spectrum. Each band was assigned to a secondary structure according to the frequency of its maximum. The area of all bands assigned to a given secondary structure was then summed and divided by the total area. This ratio gives the proportion of the polypeptide chain in that conformation (*20*). The frequency limits for each structure were first assigned according to the data determined theoretically (*25*) or experimentally (*26*): 1662−1645 cm^{-1}, α-helix; 1689−1682 and 1637−1613 cm^{-1}, *β*-sheet; 1644.5−1637 cm^{-1}, random; and 1682−1662.5 cm^{-1}, *β*-turns. These limits have been slightly adjusted to obtain a good agreement between the proportion of each structure determined by IR-ATR and X-ray crystallography (*20*). This procedure extended to a series of well-characterized proteins provided a correct estimation of the α-helix and *β*-sheet structure content with a standard deviation of 8.7% when X-ray structures were taken as a reference (*27*).

Orientation of the Secondary Structure. Attenuated total reflection infrared spectroscopy allows spectra to be recorded for ordered lipid bilayers and information to be gained about the orientation of different structures of protein or peptide (*20*, *28*). In an α-helix, the main transition dipole moment (C═O) is almost parallel to the helix axis, while in an antiparallel *β*-sheet, the polarization is opposite, predominantly perpendicular to the fiber axis (*24*). It is therefore possible to determine the mean orientation of the α-helix and *β*-sheet structures from the orientation of the peptide bond corresponding to the C═O group. Spectra were recorded with parallel (0°) and perpendicular (90°) polarized incident light with respect to the ATR plate. Polarization was expressed as the dichroic ratio R_{atr} which equals $A_{90}°/A_0°$. The mean angle between the C═O bond and a normal to the ATR plate surface is calculated from R_{atr} as described in ref *28*. The difference spectra are obtained by subtracting the 0° from the 90° polarization spectrum normalized to each other by zeroing the net integral of the intensities of the ester C═O stretching band of the Sn^{-1} and Sn^{-2} lipid chains in the 1710−1760 cm^{-1} region in the difference spectrum. The rationale behind this lies in the fact that both the Sn^{-1} and Sn^{-2} carbonyl groups are found to make angles with respect to the bilayer normal that are close to the value for an isotropic orientation and their IR intensities are therefore expected to be independent of the polarization.

Kinetics of Deuteration. This analysis was carried out as previously described (*20*). The samples were spread on a germanium plate at three different temperatures as described above. Before the deuteration was started, 10 spectra were recorded to verify the reproducibility of the measurements and the stability of the system. At time zero, a D_2O-saturated N_2 flux was applied to the sample with a flow rate of 100 mL/min that was controlled with a Brooks flow meter. The Bruker IFS55 FTIR spectrophotometer was driven by a computer program. The spectra at each time point were the accumulation of 24 scans, with a resolution of 4 cm^{-1}. The signal from atmospheric water was subtracted as described in ref *20*. The amide I and II band areas were measured between 1700 and 1600 and 1585−1502 cm^{-1}, respectively. The amide II area was divided by the amide I area for each spectrum to correct for any change in total intensity of the spectra during the deuteration process. This ratio, expressed between 0 and 100%, was plotted versus deuteration time. The 100% value is defined by the amide II:amide I ratio obtained before deuteration, whereas the 0% value corresponds to a zero absorption in the amide II region. It has been shown previously (*29*, *30*) on a series of proteins that can be fully denatured (and therefore fully deuterated) and then refolded to their native conformation that complete H−D exchange results in a 0 ± 5% absorption intensity in the amide II region. We are therefore confident that a zero absorbance in the amide II region corresponds to full deuteration of the protein.

RESULTS

Temperature-Dependent WAE-Induced Fusion of Donor Vesicles with PS/PE Target Vesicles

In this study, the fusion between peptide-coupled donor vesicles (3.5:1.5:0.25 PC/chol/PE-PDP) and target vesicles consisting of PS/PE (10:3) was investigated. Due to a lack of vesicle aggregation, mixing of these populations did not result in membrane fusion. Aggregation was accomplished however upon addition of Ca^{2+}, and the kinetics were found to be similar for each Ca^{2+} concentration that was tested, irrespective of the presence of WAE on the donor membranes (data not shown). This indicated that the kinetics of vesicle aggregation are independent of the presence of the peptide. Note that Ca^{2+} is not involved in fusion, since addition of Ca^{2+} to a suspension of peptide-devoid liposomes and target vesicles does not induce fluorescence dequenching (not shown). Hence, in this system, Ca^{2+} fulfills the function of causing membrane aggregation, while WAE serves as trigger of fusion. Fusion activity was assayed by lipid mixing (Figure 1A) or internal contents mixing (Figure 1B), and was found to depend strictly on the anchorage of WAE to donor

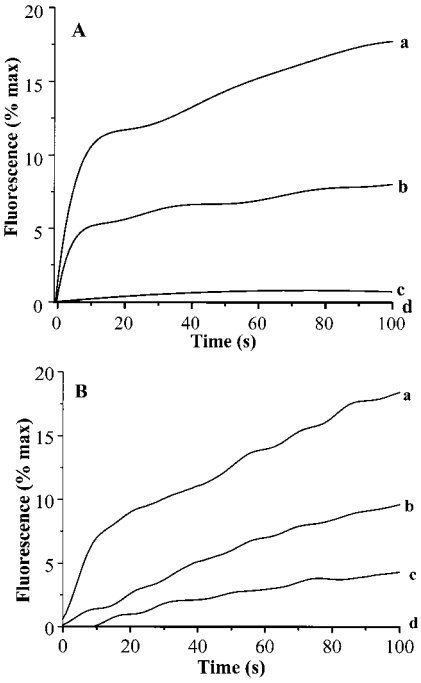

FIGURE 1: Time course of lipid and internal contents mixing upon interaction of the PS/PE target and WAE-coupled liposomes at neutral pH. (A) For lipid mixing, WAE-coupled liposomes, labeled with 1 mol % *N*-NBD-PE and 1 mol % *N*-Rh-PE, were added to PS/PE target vesicles in a lipid molar ratio of 1:6 (total lipid concentration of 70 μM). The buffer was 10 mM Tris and 150 mM NaCl at pH 7.4. The increase in *N*-NBD-PE fluorescence was recorded continuously. (B) For internal contents mixing, WAE-coupled liposomes containing $TbCl_3$ were added to DPA-loaded PS/PE vesicles in the same molar ratio that was used for the lipid mixing assay, in 10 mM Hepes, 100 mM NaCl, and 0.1 mM EDTA (pH 7.4). The following conditions were used in the experiments are depicted in both panels A and B: (a) 37 °C, (b) 20 °C, (c) 10° C, in the presence of 2 mM Ca^{2+}, and (d) 37 °C, in the absence of Ca^{2+}.

membranes. A significant change in the fluorescence signal was not seen with peptide-devoid vesicles or when the peptide was added as free monomers or between fluorescently labeled and unlabeled PS/PE vesicles (data not shown), whereas fusion was readily observed with liposomes to which WAE had been coupled (curves a−c). In the absence of Ca^{2+}, the inability of peptide-coupled vesicles to fuse with PS/PE target liposomes (curves d) is related to the fact that vesicle aggregation does not occur, as noted above. Upon the incubation temperature being raised, the initial rate of fusion rapidly increases with a maximum around 37 °C (curves a > b > c). This is in agreement with results previously obtained with PElys-containing target vesicles (*10*). Consequently, in an attempt to understand which parameters could explain the temperature dependence of fusion, we investigated structural and spatial features of the peptide anchored to a liposomal surface, in the absence and presence of target vesicles, as a function of temperature. Two different experimental approaches were used, one relying on Trp fluorescence quenching by aqueous quencher (acrylamide) and the other based on ATR-FTIR measurements.

WAE Penetration and Orientation into Donor Membranes (PC/Chol/PE-PDP LUVs)

Trp Fluorescence. It is well-established that the intrinsic fluorescence of Trp increases when the amino acid senses a more hydrophobic environment. Concomitantly, a blue shift in the emission maximum is seen (λ_{max}). These parameters were then monitored as a function of temperature for the WAE peptide anchored to a liposomal membrane, taking advantage of the N-terminal localization of its Trp residue. In solution as a free monomer, WAE exhibits a λ_{max} of 350 nm, which is characteristic of a Trp residue in a relatively nonpolar environment (*19*). The fluorescence properties of WAE after its coupling to PC/chol/PE-PDP vesicles were not markedly different.

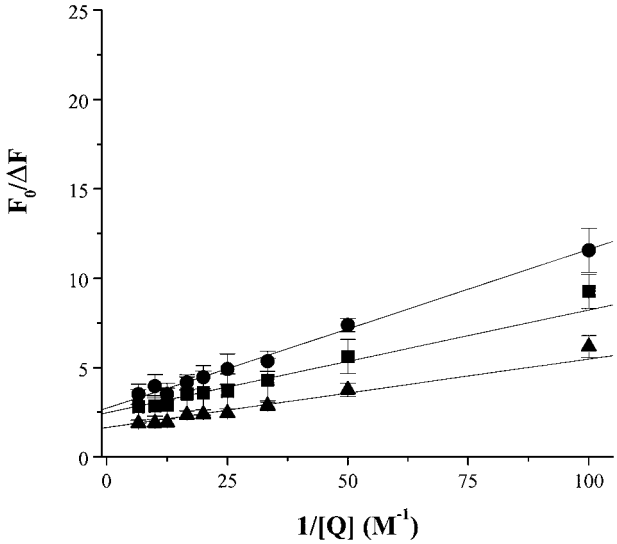

FIGURE 2: Tryptophan fluorescence quenching by acrylamide of WAE coupled to donor PC/chol liposomes in the absence of target vesicles. Peptide-coupled liposomes were preincubated for 2 min in 1 mL of buffer [10 mM Tris and 150 mM NaCl (pH 7.4)], at 10 (▲), 20 (■), or 37 °C (●), before measurement. Increasing concentrations of acrylamide (from a 3 M aqueous stock solution in buffer) were then added, and Trp fluorescence was recorded at 340 nm (λ_{exc} = 295 nm). Results are analyzed according to the modified Stern−Volmer plot (see Materials and Methods for details).

More direct information about the localization of the tryptophan can be obtained from its accessibility toward aqueous quenchers such as iodide or acrylamide that are unable to penetrate into the hydrophobic core of the lipid bilayer. Acrylamide quenching data are reflected by K_{sv}, the Stern−Volmer quenching constant, which increases when Trp is less shielded from the aqueous environment, i.e., when it faces a more hydrophilic environment. When quenching data are plotted as F_0/F versus [Q], the Stern−Volmer plot deviates from linearity, suggesting the presence of two peptide populations (data not shown). Therefore, the data were analyzed using the modified form of the Stern−Volmer equation, as described in Materials and Methods. The analysis reveals a lower accessibility to the quencher at higher temperatures (Figure 2), as determined by the slope of the curves. These data thus suggest that with increasing temperature, the peptide exhibits an increased tendency to penetrate partially into the membrane to which it is attached.

Secondary Structure Determination. The conformation of WAE coupled to the donor membrane was determined by FTIR spectroscopy. When this conformation was determined before passage of the vesicles through the Sephadex G50 column to remove uncoupled peptide, a large amide I band corresponding to two major structures, i.e., α-helix and β-sheet, is observed. This suggests the existence of two

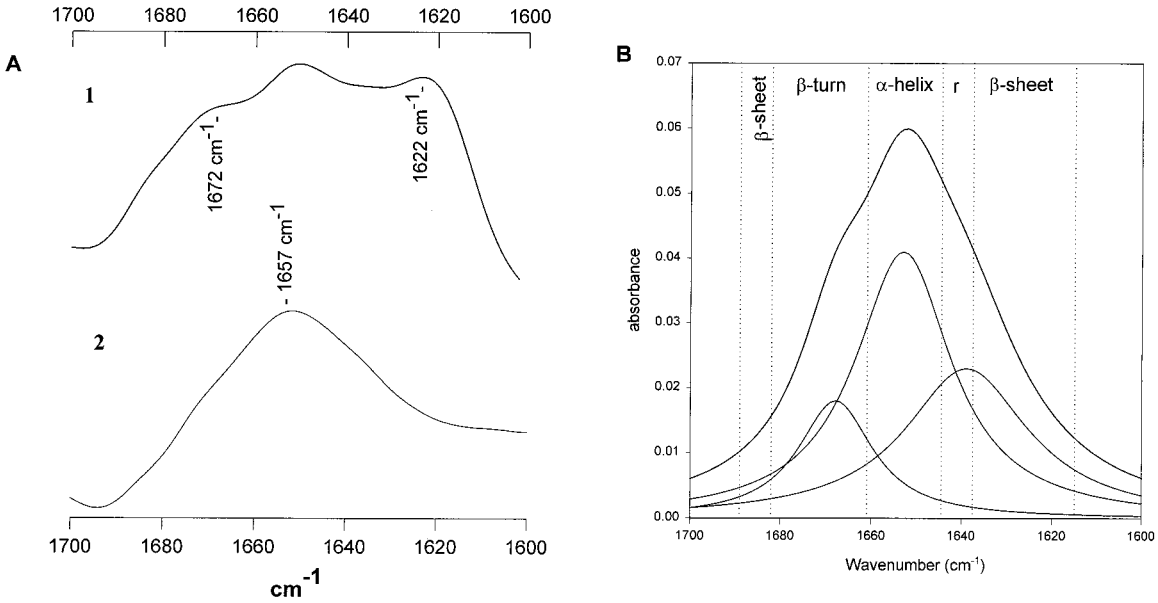

FIGURE 3: (A) Deuterated infrared spectra of WAE coupled to liposomes before (1) and after (2) passage through a PD10 column. The LPWAE was incubated for 1 h at 37 °C before being spread at the surface of the germanium plate. All spectra have been rescaled in the region between 1700 and 1600 cm^{-1} to the same amplitude. (B) Curve fitting for the amide I band of WAE coupled to PC/Chol/PE-PDP LUVs incubated at 37 °C and deuterated over the course of 2 h. The vertical dotted lines limit the regions associated with the different secondary structure.

peptide populations (Figure 3A, trace 1). Following gel chromatography, the FTIR spectra of the peptide-coupled vesicles exhibited a band centered around 1657 cm^{-1}, indicating covalently attached WAE preferentially adopted an α-helical conformation (Figure 3A, trace 2). Hence, the fraction showing the *β*-structure was evidently resulting from noncoupled peptide which, given the low wavenumber, is probably present in the aggregated state. The FTIR-ATR spectra of WAE coupled to the liposomes and spread on the germanium plate at three different temperatures were recorded in deuterated solvent. Deuteration allows the distinction between α-helical structures and random coils to be made. All three spectra look similar which suggests that no significant secondary structure change is taking place upon increasing the temperature. A quantitative analysis of the amide I band of deuterated spectra by Fourier self-deconvolution and least-squares curve fitting (*20*) allowed us to quantify the secondary structure of the peptide (Figure 3B and Table 1). For all the temperatures that were tested, the α-helical content amounted to ca. 55 ± 5%.

The above structure determination shows that WAE coupled to donor membrane mainly adopts an α-helical conformation, which is prevalent over *β*-structures, for each temperature that was tested (Table 1). This suggests that (1) the formation of α-helical structure is independent of temperature and (2) peptide helicity is not a sufficient condition for fusion to occur. Given the effect of temperature on fusion, which is not due to differences in aggregation kinetics (not shown; see ref *31*), we next examined whether temperature might affect the peptide's orientation.

Orientation of Secondary Structure. Information about the orientation of a given secondary structure can be obtained by recording ATR-FTIR peptide spectra with polarized light, provided that the peptides are oriented with respect to the internal reflection element. Figure 4 shows the 90 and 0° polarization spectra of the WAE peptide coupled to liposomes as well as the 90° minus 0° difference spectrum. A

Table 1: Estimates of the Secondary Structure and Dichroic Ratio of WAE Coupled to Donor Liposomes in the Absence (−) and Presence (+) of Target Vesicles, as a Function of Temperature

	α-helix						*β*-sheet		unordered structure (random and *β*-turn)	
temp	%[a]		R_{ATR}[b]		angle[c]		%[a]		%[a]	
(°C)	−	+	−	+	−	+	−	+	−	+
10	55	0	1.07	nd	70	−	9	80	36	20
20	52	45	1.21	2.1	60	10	16	35	32	20
37	55	47	1.35	2.2	50	10	3	32	42	21

[a] The secondary structure determination was performed from the analysis of the shape of the amide I band using a Fourier self-deconvolution curve-fitting procedure (see Materials and Methods for details). Results are means of three or four separate FTIR measurements, and the error is ±5%. [b] Dichroic ratio as indicated in Materials and Methods. [c] The angle is calculated with respect to the membrane surface normal.

coefficient was chosen to zero the lipid *ν*(C═O) band between 1700 and 1770 cm^{-1} as described previously (*20*). A positive deviation of the amide I band (between 1600 and 1700 cm^{-1}) in a polarization difference spectrum indicates an orientation of this dipole parallel to the lipid acyl chains, while a negative deviation corresponds to an orientation of the dipole perpendicular to the lipid acyl chains.

For the peptide coupled to donor vesicles and incubated at 10 °C for 1 h, a negative deviation was observed in the amide I (C═O) region of the difference spectrum (Figure 4A), whereas no deviation was observed when the peptide is incubated at 20 or 37 °C (Figure 4B). This indicates that the orientation of the α-helical structure of WAE coupled to vesicles changes with temperature. At low temperatures, the α-helix associated with the peptide lies nearly parallel to the membrane surface. An increase in the temperature modifies the orientation from parallel to an intermediate orientation, which is neither parallel nor perpendicular to the ATR element surface.

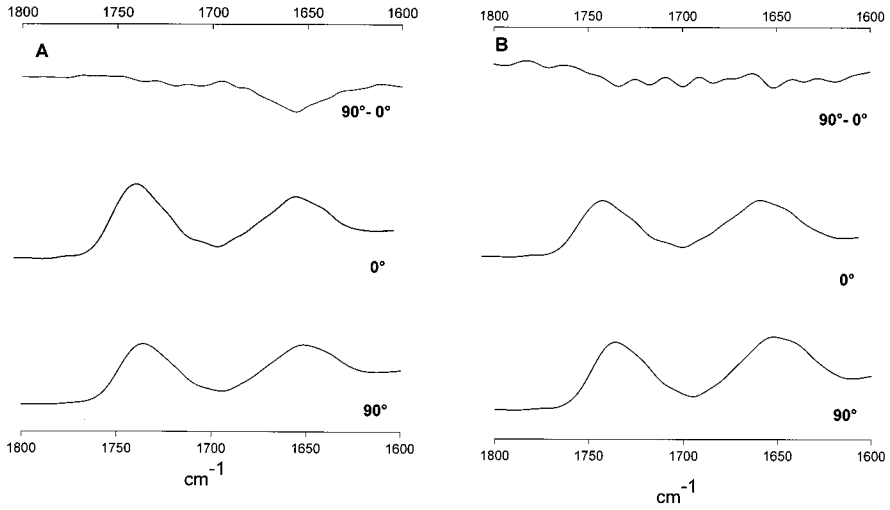

FIGURE 4: Determination of the orientation of WAE with respect to the donor membrane. Deuterated infrared spectra of WAE coupled to liposomes and incubated at 37 (A) and 10 °C (B) were recorded with incident light polarized perpendicular (90°) and parallel (0°) to the plane of the membrane. The difference spectrum (90° minus 0°) was obtained by subtracting the 0° polarized spectrum from the 90° polarized one.

The dichroic ratio of the α-helical component was calculated with the following equation (*28*):

$$R_\alpha = \frac{R - [(R+2)/(2R_{iso}+1)](1-x)}{1 - (1/R_{iso})[(R+2)/(2R_{iso}+1)](1-x)}$$

where R_α is the dichroic ratio of the α-helical component, R is the measured dichroic ratio (area of amide I at 90°/area of amide I at 0°), R_{iso} (1.52) is the ratio of the intensities at 90 and 0° of a dipole with an isotropic orientation [the ν-(C═O) being between 1763 and 1711 cm^{-1}], and x is the fraction of α-helical structure. From this dichroic ratio, it is possible to calculate a corresponding angle between the long axis of the α-helix and a normal to the germanium plate (Table 1). If the α-helical content reported in Table 1 is taken into account, the calculated dichroic ratio of 1.07 ± 0.05 corresponds to an angle of 70 ± 5° between the α-helix and a normal to the germanium plate for the peptide incubated at 10 °C, while for the peptide incubated at 20 and 37 °C, the dichroic ratios are around 1.21 ± 0.03 and 1.37 ± 0.03, corresponding to angles of 60 ± 5° and 50 ± 5°, respectively. The relationship between the dichroic ratio and the orientation of a given structure (α-helix in this case) is dependent upon the angle between the transition dipole being considered and the primary axis of the structure (*20*). The above angle is obtained with an order parameter of 1 describing the orientation of the membrane plane with respect to the germanium plate and a value of 27° for the angle between the C═O dipole and the helix axis. We note that the angles mentioned above are the maximum possible angle, because values for the order parameter of <1 or a C═O dipole−helical axis angle of >27° would decrease the calculated helix−axis membrane normal angle. Another parameter influencing the angle determination is the refractive index (n) of the film. Values of 1.7 and 1.55 are currently used for protein and lipid films, respectively (*27*). It should be kept in mind that FTIR spectroscopy does not discriminate between a fixed uniaxial orientation and the mean of two (or more) populations with different orientations corresponding to an average oblique orientation. Therefore, the results observed here are consistent with a progressive randomization of the orientation of the helical transition dipole moment as the temperature increases.

Efforts were made to characterize the orientation of the phospholipids in the bilayer to assess the overall membrane orientation on the germanium plate. This orientation is confirmed in the dichroic spectra by the negative peak observed near 1468 cm^{-1} corresponding to the δ (CH_2) peak whose transition dipole moment is perpendicular to the axis of the lipid acyl chain (data not shown). The dichroic ratio of the δ (CH_2) vibration near 1468 cm^{-1} is 0.9 ± 0.2. The corresponding mean angle between the axis of the hydrocarbon chains and a normal to the ATR plate surface was calculated from an order parameter of 1. The PC/chol/PE acyl chains make a maximum tilt of 25° with respect to the normal to the germanium surface.

Kinetics of Deuteration. To further characterize the spatial organization of the peptide and the temperature-dependent modulation of the peptide's orientation upon lipid anchorage, the kinetics of deuteration of WAE coupled to donor vesicles and incubated at different temperatures were recorded. The rate of amide hydrogen exchange with deuterium is related to the stability of the secondary structure and to the solvent accessibility to the NH amide group of the protein or peptide. Amide hydrogen exchange was followed by monitoring the amide II absorption peak [δ(N−H) with a maximum at 1544 cm^{-1}] decrease because of the shift to 1460 cm^{-1} [amide II′ δ(N−D)], as a function of the time of exposure to D_2O-saturated N_2 flow (from 15 s to 2 h; for details, see Materials and Methods).

Figure 5 represents the percentage of deuteration of coupled WAE, incubated at 10, 20, or 37 °C, which was calculated from the ratio of amide II/amide I as described in Materials and Methods. It is evident that the hydrogen−deuterium exchange is fast and important for all temperatures that were tested. However, at 10 °C, WAE undergoes a slightly faster exchange than at 20 or 37 °C, suggesting that at this temperature the peptide is slightly more accessible. However, after deuteration for 15 min, 100% of the peptide N−H had been exchanged, indicating a complete accessibility of the peptide to the solvent irrespective of the temperature.

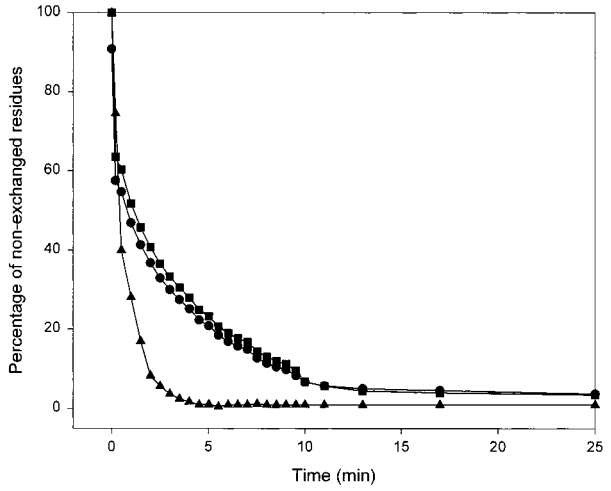

FIGURE 5: Kinetics of deuteration of WAE coupled to vesicles. Donor liposomes coupled to WAE were incubated for 1 h at 10 (▲), 20 (■), or 37 °C (●), before the sample was deposited on the germanium plate at identical temperatures. The film was exposed to a D_2O-saturated N_2 flux, and the spectra were recorded automatically as a function of time, as described in Materials and Methods. The amide II area/amide I area for each spectrum (expressed between 0 and 100%) was plotted as a function of deuteration time. Each curve is the average of two experiments.

Taken together, these results demonstrate that, although a change in the orientation of the WAE α-helix is observed when temperature increases, the peptide remains (relatively) accessible to the solvent and thus available for interacting with target bilayers. The following experiments were then designed to investigate the conformational and spatial behavior of WAE in the presence of target membranes.

WAE Penetration and Orientation into Target Membranes (PS/PE LUVs)

To study the effect of the presence of target vesicles on structural and orientational features of WAE, the peptide coupled to liposomes was incubated with PS/PE (10:3) LUVs at pH 7.2 with 2 mM Ca^{2+}, at 10, 25, or 37 °C. The interaction of WAE with target membranes was assayed by monitoring changes in intrinsic Trp fluorescence and by Trp fluorescence quenching with acrylamide. Conformational studies were performed by FTIR analysis.

Tryptophan Fluorescence. The fluorescence properties of the WAE were markedly altered upon addition of target vesicles. Their presence shifted the λ_{max} to shorter wavelengths and enhanced the intensity of fluorescence. Such changes in fluorescence properties typically occur when tryptophan enters a more hydrophobic environment, as would be the case with the penetration of WAE into the hydrophobic core of the target lipid bilayer. It must be noted that a marginal variation in Trp fluorescence quantum yield was seen in the absence of Ca^{2+}, i.e., without aggregation of the vesicles, indicating that under these conditions the Trp residue of WAE does not migrate to a hydrophobic environment (data not shown). The blue shift in λ_{max} and the enhancement of intensity were more pronounced at 37 °C than at 10 °C with a gradual decrease in λ_{max} with increasing temperature. This indicates a preferential "submersion" of WAE into the hydrophobic core of a lipid bilayer when the temperature increased. Above 20 °C, a decrease in the accessibility to acrylamide was observed (Figure 6A, ● and ■). Interestingly, at 10 °C, no change in quantum yield was seen, whereas accessibility to acrylamide is found to be lower compared to that at 20 °C, and almost similar to that obtained at 37 °C (Figure 6A, ▲).

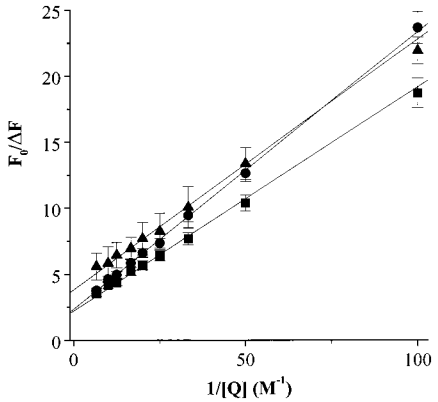

FIGURE 6: Tryptophan fluorescence quenching by acrylamide of WAE coupled to donor PC/chol liposomes in the presence of target vesicles. Peptide-coupled liposomes were preincubated for 4 min with target PS/PE vesicles at 10 (▲), 20 (■), or 37 °C (●). Increasing concentrations of acrylamide were then added, and the experiment was performed as described in legend of Figure 2.

The data are consistent with a (shallow) peptide penetration into PS/PE target membranes at elevated temperatures, like that previously demonstrated in the case of PElys-containing target vesicles (*14*). Note that these quenching experiments were performed 4 (Figure 6) or 60 min (data not shown) after addition of target vesicles. The results obtained in both cases were similar, indicating that the reaction is fast and complete within a few minutes and that the insertion of the peptide into the membrane is stable. For the following experiments, all the measurements were performed 1 h after addition of the target vesicles.

Secondary Structure Determination. Peptide secondary structure and orientation in the presence of target vesicles were further studied by ATR-FTIR. Figure 7A shows the shape of amide I in the presence of PS/PE LUVs at 10, 20, and 37 °C. At 20 and 37 °C, amide I bands were relatively broad with a maximum at 1655 cm^{-1}, suggesting the presence of α-helix. The results of amide I band analysis by Fourier self-deconvolution and least-squares curve fitting (*27*) are reported in Table 1 and show that, at 20 and 37 °C, the percentage of α-helix of the peptide is not substantially modified by the presence of target vesicles, although a slight decrease in its relative contribution was noted. However, a more detailed analysis of Table 1 reveals that the addition of PS/PE LUVs is also characterized by a slight increase in the β-sheet content and a decrease in the random content. Thus, after incubation at 10 °C, the peptide mainly adopts a β-sheet structure with a maximum absorbance at 1628 cm^{-1}, while helical structure is not apparent (Figure 7A and Table 1). As noted above, the low-frequency absorption of the β-sheet suggests that the β-strands are forming strong hydrogen bonds which may arise from intermolecular bonds formed between aggregated or oligomerized peptides (*32*). To rule out a possible artifact due to lipid absorption of target vesicles, we have recorded the spectra of liposomes of PS/PE, and the spectra exhibited no absorption band between 1700 and 1600 cm^{-1} (data not shown).

Orientation of Secondary Structure. To determine the orientation of the α-helix associated with WAE in the

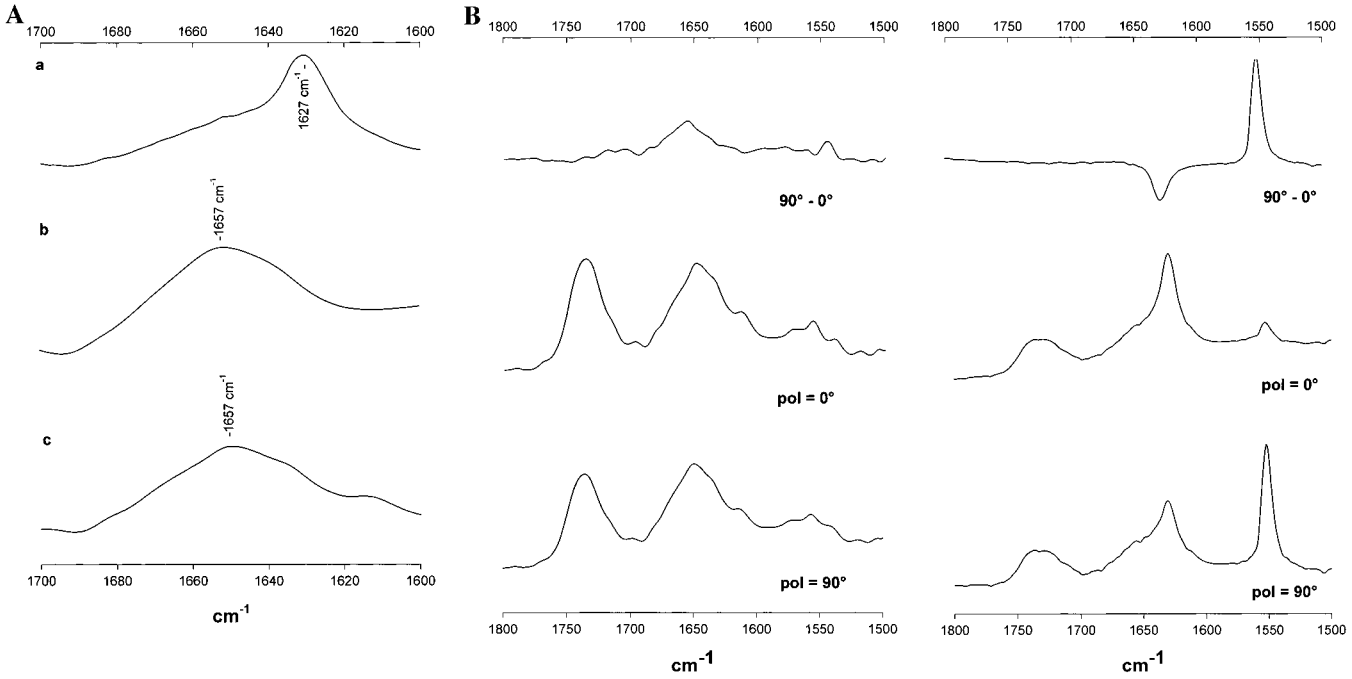

FIGURE 7: (A) Deuterated infrared spectra of WAE coupled to liposomes and incubated with target vesicles of PS/PE (1:1 donor:target ratio), at 10 (a), 20 (b), and 37 °C (c), before spreading on the germanium plate. All spectra have been rescaled in the region between 1700 and 1600 cm^{-1} to the same amplitude. (B) Determination of the orientation of WAE with respect to the target membrane. Deuterated infrared spectra of WAE coupled to liposomes incubated with target vesicles at 37 (left) and 10 °C (right) were recorded with incident light polarized perpendicular (90°) and parallel (0°) to the plane of the membrane. The difference spectrum (90° minus 0°) was obtained by subtracting the 0° polarized spectrum from the 90° polarized one.

presence of target PS/PE LUVs at 20 and 37 °C, spectra were recorded using polarized light at 90 and 0° as described above. The dichroic spectra were obtained by subtracting spectra recorded with 0° polarized light from spectra recorded with 90° polarized light. As shown in Figure 7B, a positive deviation of the dichroic spectra was present in the amide I spectral domain assigned to the α-helical structure, indicating that the α-helical component of the WAE peptide incubated at 37 and 20 °C has a transmembrane orientation. The dichroic ratio of the α-helix component was calculated using the equation described above with an R_{iso} of 1.40 which gives a value of 2.7 ± 0.1, corresponding to an angle of 10 ± 5° taking into account a 27° angle between the transition dipole and the helix axis at 37 °C, and 2.6 ± 0.1, corresponding to an angle between the α-helix and a normal to the germanium plate of 15 ± 5° at 20 °C. Thus, our data suggest that after the fusion process the α-helix of WAE is significantly more tilted than before fusion, and the result clearly demonstrates that WAE interacts strongly with the hydrophobic phase of lipid vesicles after fusion. The orientation of the β-sheet with respect to the membrane surface, observed at 10 °C, was also determined by polarized FTIR. The difference spectrum (90° minus 0°) exhibits a negative absorption at 1629 cm^{-1} and a positive peak at 1551 cm^{-1} (Figure 7B). This indicates that the C═O dipoles are preferentially oriented parallel to the membrane surface.

The organization and the conformation of the lipid molecules were studied after addition of the target vesicles. In the presence of PS/PE liposomes, the peak of the phospholipid $\omega(CH_2)$ near 1468 cm^{-1}, whose transition dipole moment is perpendicular to the axis of the lipid acyl chain, and which appears on the dichroic ratio spectra (obtained by subtracting the 0° spectrum from the 90° spectrum) as a negative deviation, demonstrates that the phospholipid acyl chains are oriented almost perpendicular to the germanium plate; i.e., the bilayer lies parallel to the germanium plate (data not shown). The dichroic ratio of the $\omega(CH_2)$ vibration at 1468 cm^{-1} is 1.00 ± 0.05, corresponding to an angle 20° with respect to the normal to the germanium surface. The addition of target vesicles to the donor does not disturb the mean orientation of the lipid molecules.

Kinetics of Deuteration. The evolution of nonexchanged residues of WAE coupled to vesicles in the presence of PS/PE LUV at 10, 20, and 37 °C as a function of deuteration time is illustrated in Figure 8. Clearly, hydrogen−deuterium exchange was faster for the WAE peptide in the absence than in the presence of the target vesicles. After deuteration for 40 min, 100% of the peptide N−H could be exchanged before fusion, suggesting a complete accessibility of the peptide to the solvent. In the presence of target vesicles at 20 and 37 °C, only 50% of the peptide NH group was exchanged, suggesting less accessibility of the peptide to the solvent. With regard the experiment performed at 10 °C, the presence of target vesicles significantly modifies the extent of H−D exchange undergone by WAE, indicating a lower accessibility to the solvent, which is entirely consistent with the Trp fluorescence quenching experiments (Figure 6; see the Discussion).

DISCUSSION

This work was aimed at gaining further insight into the molecular mechanism(s) by which a membrane-anchored peptide (WAE) induces fusion (*14*). Our model system, consisting of an 11-mer fusogenic peptide covalently coupled to liposomes, offers the unique opportunity to dissect and focus on intermediate steps along the fusion pathway, and

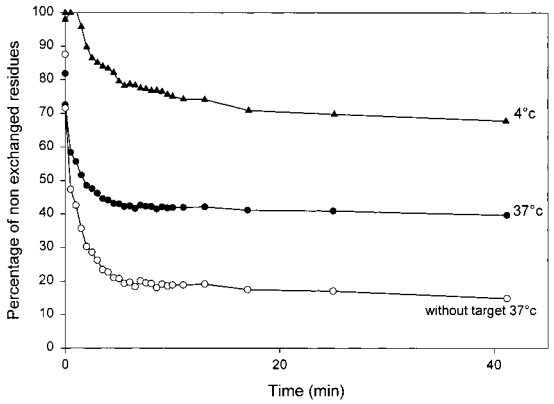

FIGURE 8: Evolution of the proportion of nonexchanged residues of WAE coupled to vesicles as a function of deuteration time. Peptide-coupled liposomes were incubated with target vesicles (black symbols) for 1 h at 10 (▲) or 37 °C (●), before sample deposition on the germanium plate. WAE-coupled liposomes (white symbols) were incubated at 37 °C in the absence of target vesicles. Each curve is the average of two experiments.

to identify the specific conformation of the peptide in a lipidic environment before, during, and after fusion. Here, spatial characteristics of WAE, i.e., secondary structure, insertion into and orientation toward lipid bilayers were investigated, in an attempt to understand the link between structural and functional aspects. The data reveal (i) an insertion of the peptide as an oriented α-helix into the target membrane, under fusogenic conditions; and (ii) conversely a lack of membrane insertion and a predominant *β*-sheet structure of the peptide under nonfusogenic conditions (low temperatures). Evidence was obtained which suggests that the folding of WAE into an α-helix, together with previously described molecular shape features (*31*), governs the ability of WAE to submerge into the target membrane. This work therefore suggests that insertion of WAE into the target membrane, according to spatially well-defined criteria, represents a key triggering event in peptide-induced fusion, presumably leading to "controlled" membrane destabilization (*33*, *34*).

Temperature Regulates Peptide-Induced Fusion through an Effect on Peptide Penetration. The temperature dependence of various fusion reactions has been widely demonstrated, in both biological fusion systems (*35*−*37*) and protein- or peptide-induced fusion of model membranes (*10*, *38*). Since the extent of lateral diffusion of lipids in biological membranes decreases with temperature, fusion could be retarded at the step of hemifusion, due to a stabilization of the highly bent lipid intermediates (*35*). More likely, however, the inhibitory effect of (low) temperature may be related to a reduced mobility of membrane-associated fusion proteins (*36*, *39*) as regulated by their lipid-surrounded anchorage domain (*40*). Consequently, the rate of fusion decreases, presumably due to alterations in the formation or rate of formation of fusion complex (*36*, *41*, *42*). Interestingly, the rate of WAE-induced fusion is also strongly reduced at low temperatures with a concomitant decrease in the rate of peptide complex formation. The formation of this complex could be relevant to fusion (*31*). This prompted us to further investigate whether a relationship could exist between temperature, peptide penetration, and peptide-induced fusion. The ability of WAE to penetrate into PS/PE target membranes as a function of temperature was assessed by monitoring the accessibility of its Trp residue to quenching by acrylamide and the accessibility of the whole peptide molecule to D_2O. The data reveal unambiguously that an *increase* in temperature is accompanied by a *decrease* in accessibility of Trp to acrylamide (Figure 6), i.e., a facilitated insertion of the peptide into the hydrophobic core of the target bilayer. Most intriguingly, a *decrease* in temperature was not accompanied by an *increased* accessibility of WAE to either acrylamide or D_2O, and thus seemingly "more inserted" into the target bilayer than at higher temperatures. This is not in agreement with the observed red shifts and decrease in quantum yield, typical for a hydrophobic exposure of the peptide.

Therefore, although a relation between temperature, penetration, and fusion seems to exist at elevated temperatures, no obvious correlation can be found at low temperatures. It would thus appear that an additional factor(s) such as secondary structure and/or orientation of WAE toward its own membrane or toward the target membrane may be a key regulating parameter in this respect.

Peptide Penetration Is Closely Related to Peptide Structure and Modulates Fusion. In an attempt to clarify peptide dynamics at low temperatures, we have studied the structure and mode of insertion of WAE coupled to donor vesicles, under fusogenic conditions (high temperatures and in the presence of target vesicles) and nonfusogenic conditions (low temperatures and/or in the absence of target vesicles).

Under fusogenic conditions (Figure 1), WAE was found to insert into the target PS/PE membranes as a sided α-helix (Figure 7A and Table 1), which is also the conformation adopted by the peptide in the absence of target vesicles (Figure 3 and Table 1; see also ref *15*). This result is in line with the abundant literature suggesting that α-helix is the fusion-permissive conformation (*9*, and references therein, *43*), although this has been questioned recently (*45*, *46*). At low temperatures and in the presence of target vesicles, the peptide undergoes a conformational change from an α-helix to an aggregated *β*-sheet (Figure 7A and Table 1), which is no longer able to insert into the target bilayer and lies flat on the membrane surface (Figure 7B). This novel finding gives thus consistency to the aforementioned decreased accessibility to acrylamide and D_2O, and is readily explained by the more compact shape adopted by the peptide due to aggregation between molecules at the liposome surface. Most importantly, this conformational change is entirely reversible when the 10 °C-incubated sample is heated to 37 °C, and the fusion signal is fully recovered (I. Martin and E.-I. Pécheur, unpublished observations).

Taken together, these data support a prominent role of the α-helical conformation in conveying fusogenicity to a fusion peptide. In addition, this agrees well with the view that *β*-sheet structures are inhibitory to fusion (*47*), which, as revealed in the work presented here, is due to a lack of embedment in the target membrane and thus a lack of area expansion around the contact site (*48*). It must be noted here that in most studies in which conclusions were drawn about a prevalence of *β*- over α-structures in driving fusion, the lipid-to-peptide ratio used was low (<60), and/or membrane-bound peptide was not separated from unbound peptide before measurements were taken (*45*, *49*), leading to an overestimation of the amount of *β*-structures. An important finding of this study is the unambiguous demonstration that

the peptide penetration and peptide-induced fusion are correlated, as evidenced by results obtained at low temperatures (Figures 1 and 7A,B).

Peptide Orientation toward Membranes and Its Significance for Fusion. In the absence of target vesicles, FTIR measurements revealed that the peptide anchorage to the liposomal surface constrained WAE to adopt an α-helical conformation at high (*14*) and low temperatures (Figure 3 and Table 1). Its accessibility to acrylamide and D_2O was found to decrease when temperature increases (Figures 2 and 5), and its orientation changed from parallel to the surface at low temperatures to a more oblique orientation and >20 °C (Figure 4 and Table 1). This suggests a greater flexibility of the peptide molecule at higher temperatures, probably allowing the insertion of the peptide into its own membrane (cf. Figures 2 and 5) (as also supported by experiments using spin-labeled probes in the donor membrane, E.-I. Pécheur and D. Hoekstra, unpublished observations). This picture changes dramatically in the presence of target membranes, since the α-helix of WAE embeds in the target bilayer more deeply than in its own membrane (compare Figure 2 with Figure 6, and Figure 5 with Figure 8), and at a slightly tiled angle with respect to lipid acyl chains.

When our model system is considered, it is evident that insertion and the mode of insertion of WAE into target membranes depend strongly on (i) the anchorage of the peptide, which induces geometrical constraints; (ii) the secondary structure of the peptide, as a consequence of anchorage; and (iii) the flexibility of the peptide. WAE-induced fusion proceeds likely through the formation of highly bent lipid intermediates or stalks (*14*). The ability of the peptide to induce such structures will likely depend on its insertion into the target membrane. It is thus plausible that the angle of insertion of WAE, in conjunction with its wedge-like geometry (*31*), will force lipids to tilt, thereby promoting stalk formation. The flexibility of the peptide on the liposomal surface, only observed under fusogenic conditions, could then facilitate peptide−peptide interactions underlying the phenomenon of peptide clustering also related to fusion (*31*). Finally, considering that insertion of WAE into its own membrane does not occur at low temperatures where little fusion is observed, we find it is tempting to suggest that (shallow) penetration of WAE into its own membrane, through the destabilization it creates, could be a step toward the lipid destabilization propagated to the target membrane and leading to fusion. This hypothesis gains further support in light of most recent work from Chernomordik and co-workers (*50*). The significance of such a behavior in our model system remains to be determined, but the use of a model composed of a membrane-anchored peptide could help in gaining a further understanding of the mechanism(s) of fusion.

REFERENCES

1. Chernomordik, L. (1996) *Chem. Phys. Lipids 81*, 203.
2. Duzgunes, N. (1985) *Subcell. Biochem. 11*, 195.
3. Zimmerberg, J., Curran, M., and Cohen, F. S. (1991) *Ann. N.Y. Acad. Sci. 635*, 307.
4. Monck, J. R., and Fernandez, J. M. (1994) *Neuron 12*, 707.
5. Gaudin, Y., Tuffereau, C., Durrer, P., Flamand, A., and Ruigrok, R. W. (1995) *J. Virol. 69*, 5528.
6. White, J. M. (1990) *Annu. Rev. Physiol. 52*, 675.
7. Wolfsberg, T. G., and White, J. M. (1996) *Dev. Biol. 180*, 389.
8. Myles, D. G., and Primakoff, P. (1997) *Biol. Reprod. 56*, 320.
9. Durell, S. R., Martin, I., Ruysschaert, J. M., Shai, Y., and Blumenthal, R. (1997) *Mol. Membr. Biol. 14*, 97.
10. Pécheur, E.-I., Sainte- Marie, J., Bienvenue, A., and Hoekstra, D. (1999) *J. Membr. Biol*. (in press).
11. Wharton, S. A., Martin, S. R., Ruigrok, R., Skehel, J. J., and Wiley, D. C. (1988) *J. Gen. Virol. 69*, 1847.
12. Lear, J. D., and Degrado, W. F. (1987) *J. Biol. Chem. 262*, 6500.
13. Murata, M., Takahashi, S., Kagiwada, S., Suzuki, A., and Ohnishi, S. (1992) *Biochemistry 31*, 1986.
14. Pécheur, E.-I., Hoekstra, D., Sainte- Marie, J., Maurin, L., Bienvenue, A., and Philippot, J. R. (1997) *Biochemistry 36*, 3773.
15. Pécheur, E.-I., Martin, I., Ruysschaert, J. M., Bienvenue, A., and Hoekstra, D. (1998) *Biochemistry 37*, 2361.
16. Mrsny, R. J., Volwerk, J. J., and Griffith, O. H. (1986) *Chem. Phys. Lipids 39*, 185.
17. Struck, D. K., Hoekstra, D., and Pagano, R. E. (1981) *Biochemistry 20*, 4093.
18. Wilschut, J., Duzgunes, N., Fraley, R., and Papahadjopoulos, D. (1980) *Biochemistry 19*, 6011.
19. Keating, N. S., Cherek, H., and Lakowicz, J. R. (1985) *Anal. Biochem. 148*, 349.
20. Goormaghtigh, E., Cabiaux, V., and Ruysschaert, J. M. (1994) *Subcell. Biochem. 23*, 329.
21. Cortijo, M., Alonso, A., Gomez, F. J., and Chapman, D. (1982) *J. Mol. Biol. 157*, 597.
22. de-Jongh, H. H., Goormaghtigh, E., and Ruysschaert, J. M. (1996) *Anal. Biochem. 242*, 95.
23. Fringeli, U. P., and Günthard, H. H. (1981) *Mol. Biol. Biochem. Biophys. 31*, 270.
24. Gremlich, H. U., Fringeli, U. P., and Schwyzer, R. (1984) *Biochemistry 23*, 1808.
25. Krimm, S., and Bandekar, J. (1986) *Adv. Protein Chem. 38*, 181−364.
26. Byler, D. M., and Susi, H. (1986) *Biopolymers 25*, 469.
27. Goormaghtigh, E., Cabiaux, V., and Ruysschaert, J. M. (1990) *Eur. J. Biochem. 193*, 409.
28. Raussens, V., Ruysschaert, J. M., and Goormaghtigh, E. (1997) *J. Biol. Chem. 272*, 262.
29. de-Jongh, H. H., Goormaghtigh, E., and Ruysschaert, J. M. (1995) *Biochemistry 34*, 172.
30. Raussens, V., Narayanaswami, V., Goormaghtigh, E., Ryan, R. O., and Ruysschaert, J. M. (1996) *J. Biol. Chem. 271*, 23089.
31. Pécheur, E.-I., Sainte-Marie, J., Bienvenue, A., and Hoekstra, D. (1999) *Biochemistry 38*, 364.
32. Jackson, M., and Mantsch, H. H. (1995) *Crit. Rev. Biochem. Mol. Biol. 30*, 95.
33. Epand, R. M., and Lim, W. (1995) *Biosci. Rep. 15*, 151.
34. Hernandez, L. D., Hoffman, L. R., Wolfsberg, T. G., and White, J. M. (1996) *Annu. Rev. Cell Dev. Biol. 12*, 627.
35. Chernomordik, L. V., Frolov, V. A., Leikina, E., Bronk, P., and Zimmerberg, J. (1998) *J. Cell Biol. 140*, 1369.
36. Hoekstra, D., and Kok, J. W. (1989) *Biosci. Rep. 9*, 273.
37. Stegmann, T., White, J. M., and Helenius, A. (1990) *EMBO J. 9*, 4231.
38. Ulrich, A. S., Otter, M., Glabe, C. G., and Hoekstra, D. (1998) *J. Biol. Chem. 273*, 16748.
39. Lee, P. M., Cherry, R. J., and Bachi, T. (1983) *Virology 128*, 65.
40. Edidin, M., Zuniga, M. C., and Sheetz, M. P. (1994) *Proc. Natl. Acad. Sci U.S.A. 91*, 3378.
41. Gutman, O., Danieli, T., White, J. M., and Henis, Y. I. (1993) *Biochemistry 32*, 101.
42. Henis, Y. I., Herman, B. Y., Aroeti, B., and Gutman, O. (1989) *J. Biol. Chem. 264*, 17119.
43. Martin, I., Schaal, H., Scheid, A., and Ruysschaert, J. M. (1996) *J. Virol. 70*, 298.

44. Martin, I., Dubois, M. C., Defrise-Quertain, F., Saermark, T., Burny, A., Brasseur, R., and Ruysschaert, J. M. (1994) *J. Virol. 68*, 1139.
45. Muga, A., Neugebauer, W., Hirama, T., and Surewicz, W. K. (1994) *Biochemistry 33*, 4444.
46. Pereira, F. B., Goni, F. M., and Nieva, J. L. (1997) *AIDS Res. Hum. Retroviruses 13*, 1203.
47. Gray, C., Tatulian, S. A., Wharton, S. A., and Tamm, L. K. (1996) *Biophys. J. 70*, 2275.
48. Novick, S. L., and Hoekstra, D. (1988) *Proc. Natl. Acad. Sci. U.S.A. 85*, 7433.
49. Rodriguez-Crespo, I., Gomez, G. C., Encinar, J. A., Gonzalez, R. J., Albar, J. P., Peterson, D. L., and Gavilanes, F. (1996) *Eur. J. Biochem. 242*, 243.
50. Kozlov, M. M., and Chernomordik, L. (1998) *Biophys. J. 75*, 1384.

BI9829534